

Spin preservation of a Ni adatom on amorphous graphene

Hongbo Du,¹ Kaige Hu¹,² Chongze Wang,³ Haifeng Li,¹ Guohua Xu,¹ Lingmin Yu¹,⁴ J. Cho,^{5,*} and Yu Jia^{5,6,7,†}

¹Department of Physics, School of Science, Xi'an Technological University, Xi'an, Shaanxi 710032, China

²Department of Physics, School of Physics and Optoelectronic Engineering, Guangdong University of Technology, Guangzhou 510006, China

³Department of Physics and Research Institute for Natural Science, Hanyang University, 222 Wangsimni-ro, Seongdong-Ku, Seoul 04763, Republic of Korea

⁴School of Materials, Xi'an Technological University, Xi'an, Shaanxi 710032, China

⁵Joint Center for Theoretical Physics, School of Physics and Electronics, Henan University, Kaifeng 475004, People's Republic of China

⁶Key Laboratory for Special Functional Materials of Ministry of Education, and School of Physics and Electronics, Henan University, Kaifeng 475001, China

⁷Institute of Quantum Materials and Physics, Henan Academy of Sciences, Zhengzhou 450046, China



(Received 20 November 2023; revised 4 February 2024; accepted 6 February 2024; published 21 February 2024)

Two-dimensional amorphous materials can be regarded as electronic systems with a combination of amorphous and dimensional confinement effects that contributes to the discrete localized tail states near the Fermi level. In general, the magnetic properties of magnetic atoms may not be preserved upon doping into nonmagnetic metals or adsorbing onto their surfaces, e.g., Ni atoms adsorbed onto nonmagnetic metal or semiconductor surfaces. Earlier experimental and theoretical studies showed that as a Ni atom adsorbed on pristine graphene, the magnetic moment completely disappeared. Here, using first-principles calculations, we investigate the structural and magnetic properties of Ni single atom and dimer adsorbed on amorphous graphene (AG). We find that the carbon eight-member ring in AG gives rise to the most stable adsorption site for Ni adatoms and that the spin moments of adsorbed Ni single atom and dimer can be partially preserved. The mechanism of this spin preservation of Ni adatoms can be understood in terms of the disorder-induced localization and its tight-binding model. Such a localization effect due to the disordered lattice of AG weakens the hybridization between the Ni *d*- and graphene π orbitals, thereby leading to a preservation of spin moment in Ni adatoms. Our findings offer promise for many applications such as single-atom catalysis and spintronic devices.

DOI: [10.1103/PhysRevB.109.075425](https://doi.org/10.1103/PhysRevB.109.075425)

I. INTRODUCTION

Amorphous materials have short- and medium-range orders that can be similar to the basic structural units found in the corresponding crystalline phase of the same compound and thus still preserve some of the physical properties of the crystalline phase. Meanwhile, they have also been verified to exhibit distinctive properties that were not observed in crystalline structures [1–5]. Carbon-based materials involve diverse allotropes such as diamond with sp^3 hybridization, graphite (graphene and fullerene) with sp^2 hybridization, and graphyne with mixed sp^2 and sp hybridization. While these carbon-based crystalline materials have been actively investigated, the synthesis of high-quality amorphous carbon remains a challenge. Recently, millimeter-sized, nearly pure sp^3 amorphous carbon was synthesized by heating the fullerene at pressures close to the cage-collapse boundary [6]. This sp^3 amorphous carbon exhibits superior mechanical and thermal properties and optical transparency, together with tunable band gaps. Therefore, the experimental and theoretical research on amorphous carbon thin films has been increasing significantly in recent years. Specifically, the controllable synthesis of ultrathin films gives rise to intriguing physical

properties that can be utilized for electronic and electrochemical applications.

In 2020, a large-area, freestanding monolayer of sp^2 amorphous carbon film was first synthesized by laser-assisted chemical vapor deposition (CVD) [7]. This freestanding amorphous carbon monolayer was not a Zachariasen continuous random network but resembled the competing crystalline model [7]. The stable amorphous graphene (AG) films directly grown on various surfaces at low temperatures are useful for a wide range of applications, including anti-corrosion barriers for heat-assisted magnetic recording on magnetic hard disks and current collectors–electrodes in batteries and supercapacitors. Recently, amorphous graphite has been theoretically proposed by Thapa *et al.* [8] using *ab initio* molecular dynamics simulation, stimulating the achievement of experimental synthesis. Such layered amorphous graphite may enable the realization of monolayer AG via exfoliation. Indeed, recent studies of carbon or boron nitride amorphous monolayers [9] showed that elemental amorphous graphene formed the crystallite-containing Zachariasen continuous random networks, while the amorphous BN monolayer preferred compositionally disordered pseudo-Zachariasen continuous random networks. More recently, amorphous carbon monolayers with distinct degrees of disorder and electrical conductivity were synthesized by using heteroaromatic precursors in thermal chemical vapor

*jcho@henu.edu.cn

†jiayu@zzu.edu.cn

deposition (CVD) [10]. A facile tuning of the degrees of disorder and electrical conductivity in amorphous carbon monolayers was reported using varying growth temperatures.

Graphene is considered a prototypical substrate that can be useful for single-atom catalysts [11,12]. It is generally required that substrates provide a sufficient bonding to adatoms but hardly alter the intrinsic physical and chemical properties of adsorbed atoms or clusters. While graphite is known to be inert to some extent, with the physical and chemical properties of adatoms, the metal atoms on pristine graphene can migrate easily and then aggregate to form clusters or even large nanoparticles as temperature increases [13,14]. Thus, defective graphene has been often used to improve the stability of adatoms [15,16]. AG may also be a good substrate for adatoms because of its disordered structure. Five-, six-, seven-, and eight-member rings are common units composing AG. Complex structures of AG may provide distinct novel properties compared to pristine graphene. Specifically, the measured proton permeability of AG becomes ~ 1000 times higher than that of pristine graphene; lithium ions can also permeate through AG, while they cannot permeate through pristine graphene [17].

Magnetic properties of adatoms on substrates are essential ingredients in spintronics applications [18]. In general, the magnetic properties of magnetic atoms may not be preserved upon doping into nonmagnetic metals or adsorbing onto their surfaces. For example, Ni atoms adsorbed on nonmagnetic metal or semiconductor surfaces [19,20] lose a spin moment, which can be explained by the disorder-induced $s-d$ interaction model [20]; the magnetic properties of Ni atoms completely disappear on pristine graphene [21]. Therefore, preserving the magnetic properties of adsorbed atoms on substrates becomes a very important issue in surface science.

For amorphous semiconductors, electronic states can be classified into the extended and localized states in the central and tail regions of the energy band around the Fermi level, respectively. Here, electrons in the localized states are confined to a specific region [22,23], which is called Anderson localization [19,24,25]. Specifically, two-dimensional amorphous systems feature a combination of amorphous and dimensional confinement effects, and give rise to a transition from a continuous distribution of electron tail states to discrete levels. Therefore, the localized effects, combined with the disorder arrangement, can contribute to the novel electronic behavior in two-dimensional amorphous systems. As the most basic form of two-dimensional amorphous structure, amorphous graphene has been successfully synthesized by various experimental techniques [7,10]. In this work, using first-principles calculations, we investigate the adsorption of Ni single atom and dimer on AG as a model system to explore how amorphous structures influence the magnetic moment of Ni adatoms. It is revealed that the spin moments of Ni adatoms on AG can be partially preserved, therefore offering a practical approach to modulating the magnetic moments of adatoms in amorphous materials.

II. MODEL AND COMPUTATIONAL METHODS

Our first-principles density-functional theory (DFT) calculations were performed using the Vienna *Ab initio*

Simulation Package with the projector-augmented wave method [26,27]. For the exchange-correlation energy, we employed the generalized-gradient approximation functional of Perdew-Burke-Ernzerhof [28]. The Hubbard parameter $U_{\text{eff}} = 2.5$ eV for Ni $3d$ orbitals [29] was considered using Dudarev's approach [30]. Using *ab initio* molecular dynamics simulation, we predicted AG with a carbon density range of about 2.3 g/cm^3 and periodic boundary conditions [8]. We constructed many samples with 64–256 random distributions of carbon atoms in a box as an initial structure of our model. Then, the system evolved at $T = 3000$ K using the canonical ensemble with a Nosé-Hoover thermostat [31,32] in a simulation time of about 100 ps. The plane-wave basis was employed with a kinetic energy cutoff of 520 eV. The structural optimization was done by using the Γ point [33], while the density of states (DOS) and charge density of AG were calculated with the Monkhorst-Pack k meshes of $3 \times 3 \times 1$. All structural configurations were fully optimized with the convergence energy and force criteria less than 1×10^{-6} eV and 0.01 eV/\AA , respectively. The van der Waals interaction was included using the DFT-D3 scheme [34]. We calculated the adsorption energy E_{ads} with the formula

$$E_{\text{ads}} = E_{\text{sub}} + E_{\text{ad}} - E_{\text{total}} \quad (1)$$

where E_{sub} is the total energy of the substrate (pristine graphene or AG), E_{ad} is the total energy of adsorbate (isolated Ni single atom or dimer), and E_{total} is the total energy of Ni adatoms on the substrate. Energy barriers of Ni-atom migration between the different sites on AG were calculated using the climbing-image nudged elastic band method [35,36]. To simulate the adsorption of Ni single atom and dimer on AG, we chose a supercell with 118 carbon atoms, as shown in Fig. 1(a).

III. RESULTS AND DISCUSSION

A. Structures of Ni single atom and dimer adsorbed on AG

We first consider a Ni single atom adsorbed on AG. Figure 1(a) shows the optimized structure of a free-standing AG layer, which is composed of five-, six-, seven-, and eight-member rings with sp^2 hybridization. The pair-correlation functions of AG and pristine graphene are displayed in Fig. 1(b). The broad peaks in the pair-correlation function of AG reflect its amorphous character. For the five- and six-member rings, Ni adatom prefers adsorption at the hollow site [denoted as S_1 and S_2 in Fig. 1(a)], while for the seven-member ring, the adsorption site is near a hollow site which is slightly off the other hollow site (denoted as S_3). For the eight-member ring, the Ni adatom prefers adsorption at the bridge site (denoted as S_4). Therefore, the adsorption site of Ni adatom shifts from the hollow site to the bridge site with increasing the size of the carbon ring. On pristine graphene, there are three possible adsorption sites of a Ni single atom: i.e., (1) the top site directly above a carbon atom, (2) the bridge site directly over the bond between two carbon atoms, and (3) the hollow site centered over a hexagon carbon ring. We find that the most stable adsorption site of a Ni single atom on pristine graphene is the hollow site, in good agreement with previous DFT calculations [13,21].

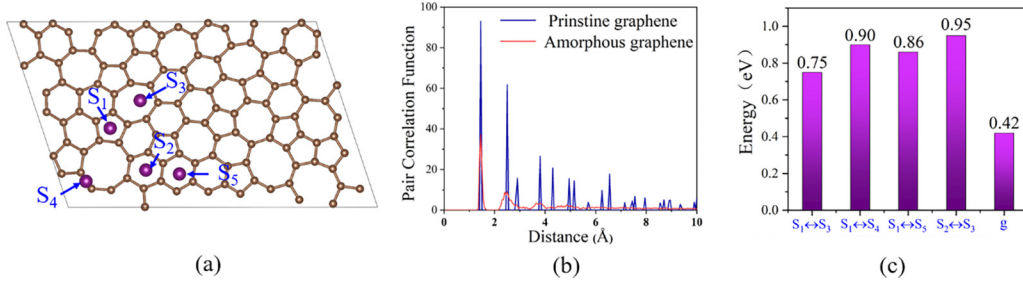


FIG. 1. (a) Zero-pressure relaxed structure of AG after 100 ps at 3000 K, obtained using first-principles molecular dynamics simulations with the canonical ensemble. The stable adsorption sites of Ni single adatom on AG are denoted as S_1 , S_2 , S_3 , S_4 , and S_5 . (b) Pair-correlation functions of AG and pristine graphene. (c) Migration energies of Ni adatom between the positions shown in (a). The migration energy between the centers of nearest-neighboring six-member rings in pristine graphene is denoted as “g.”

The adsorption energies of Ni adatoms at the adsorption sites S_1 , S_2 , S_3 , and S_4 are calculated to be 1.54, 1.47, 1.23, and 1.75 eV, respectively (see Table I). Therefore, the most stable adsorption site is the bridge site of the eight-member ring, and its adsorption energy is much larger than that (0.87 eV) on pristine graphene. Here, the Ni–C bond length $d_{\text{Ni-C}}$ at the bridge site of the eight-member ring is 1.90 Å, shorter than that (2.10 Å) at the hollow site on pristine graphene (see Table I). This result indicates that the Ni–C bond on AG has a more covalent character than that on pristine graphene, as discussed below. It is noted that $d_{\text{Ni-C}}$ in the eight-member ring also is shorter than the corresponding values in the five-, six-, and seven-member rings (see Table I). However, although the Ni adatom in the seven-member ring has the smallest adsorption energy, its value of $d_{\text{Ni-C}}$ (2.06 Å) is slightly smaller than those in the five- and six-member

rings. Note that the number of Ni–C bonds in the seven-member ring is four while those in the five- and six-member rings are five and six, respectively. Therefore, the shorter Ni–C bond length in the seven-member ring is likely due to the reduced number of Ni–C bonds.

Figure 1(c) shows the calculated migration energies of a Ni single atom on AG, together with the corresponding values on pristine graphene. We find that the migration energies between neighboring different carbon rings on AG range from 0.75 to 0.95 eV, which is much higher than that (0.42 eV) between neighboring six-member rings on pristine graphene. This result indicates that the Ni adatom on AG can be more thermodynamically stable than the Ni adatom on pristine graphene, consistent with their calculated adsorption energies (see Table I).

TABLE I. Calculated adsorption energy E_{ads} (in eV) and bond lengths $d_{\text{Ni-C}}$ and $d_{\text{Ni-Ni}}$ (in Å) of Ni single atom and dimer at the various adsorption sites (see Figs. 1 and 2) on AG and pristine graphene (PG). The most stable adsorption site of Ni single atom on PG is the hollow site of the six-member ring. The P and V in the parentheses represent the adsorption configurations of Ni dimer attached parallel and vertical to the substrate, respectively. The adsorption sites for Ni dimer vertical to the substrate are the same as those for Ni single atom.

	Site	E_{ads}	$d_{\text{Ni-C}}$	$d_{\text{Ni-Ni}}$
Single/AG	S_1	1.54	2.08	
	S_2	1.47	2.15	
	S_3	1.23	2.06	
	S_4	1.75	1.90	
Single/PG	Hollow	0.87	2.10	
Dimer (P)/AG	D_1	2.94	2.10	2.30
	D_2	2.75	2.11	2.39
	D_3	2.96	2.03	2.37
	D_4	3.40	2.01	2.30
Dimer(P)/PG	D_g	2.13	2.13	2.40
Dimer (P)/AG	S_1	3.15	2.18	2.20
	S_2	3.06	2.26	2.13
	S_3	2.92	2.18	2.23
	S_4	3.18	2.03	2.15
Dimer(V)/PG	Hollow	2.75	2.26	2.21

Next, we consider a Ni dimer adsorbed on AG. There are two species of adsorption configurations with the Ni dimer either lying parallel to the AG sheet or standing up. Figures 2(a)–2(d) display four different Ni-dimer adsorption sites parallel to the AG sheet. Figure 2(a) is the local minimum structure of Ni dimer crossing the five- and six-member rings (denoted as D_1); Fig. 2(b), crossing two neighboring six-member rings (D_2); Fig. 2(c), crossing neighboring five- and seven-member rings (D_3); Fig. 2(d), residing within the eight-member ring (D_4). For comparison, Fig. 2(e) shows the adsorption configuration of a Ni dimer on pristine graphene, where two Ni atoms are located near the hollow sites of the neighboring six-member rings (D_g). Table I summarizes the calculated adsorption energies of various Ni-dimer adsorption configurations parallel to the AG sheet. We find that the adsorption configurations D_1 , D_2 , D_3 , and D_4 have adsorption energies of 2.94, 2.75, 2.96, and 3.40 eV, respectively. It is worth noting that these adsorption configurations on AG are significantly larger in adsorption energy than that (2.13 eV) of an adsorbed Ni dimer parallel to pristine graphene, indicating that the Ni dimer is more strongly bound to AG compared to pristine graphene.

For an adsorbed Ni dimer perpendicular to the AG sheet, the stable adsorption sites are the same as those of a Ni single atom [see Fig. 1(a)]. The adsorption energy and the bond lengths $d_{\text{Ni-C}}$ and $d_{\text{Ni-Ni}}$ for each Ni-dimer adsorption configuration are summarized in Table I. We find that a Ni dimer adsorbed near the eight-member ring has an adsorption energy of 3.18 eV, larger than those of other adsorption configurations (see Table I). Among all the Ni-dimer adsorption

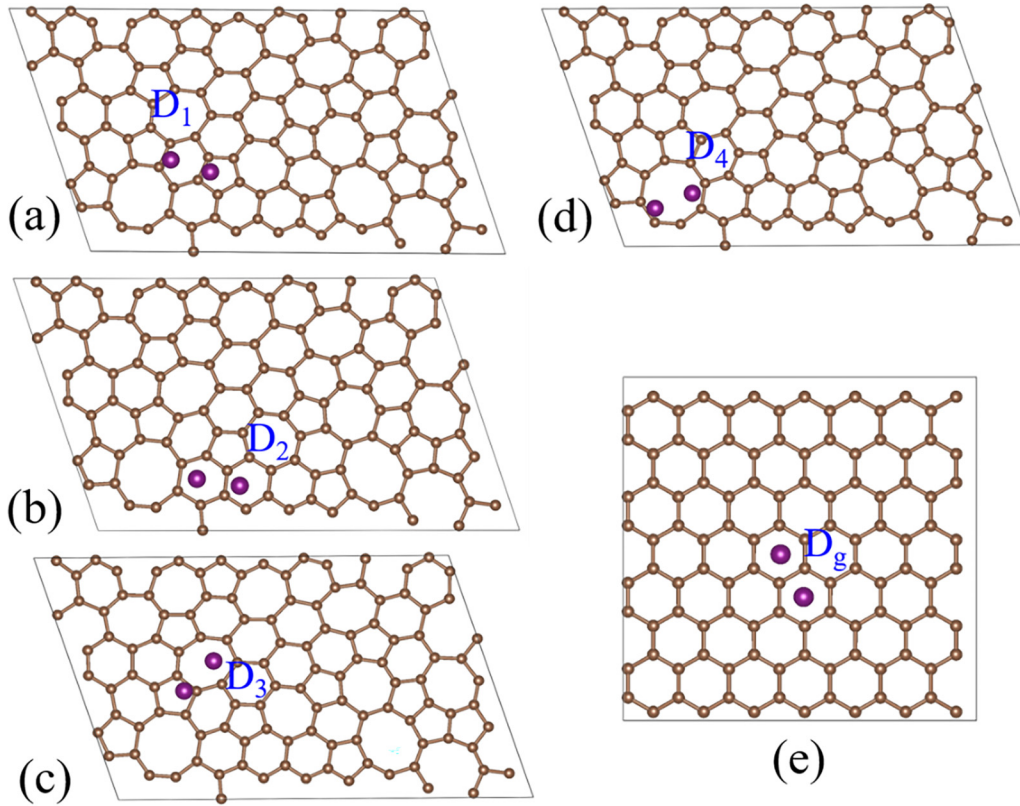


FIG. 2. (a)–(d) Various adsorption configurations of a Ni dimer on AG. The stable adsorption sites of Ni dimer on AG are denoted as D_1 , D_2 , D_3 , and D_4 . The most stable adsorption configuration D_g of a Ni dimer on pristine graphene is given in (e). Here, all the Ni dimers lie parallel to the graphene sheet.

configurations, the adsorbed Ni dimer parallel to the AG sheet within the eight-member ring [i.e., D_4 in Fig. 2(d)] is the most stable. It is thus concluded that the eight-member ring in AG plays a crucial role in stabilizing the adsorption of both a Ni single atom and dimer. Our optimized AG structure shows that the concentration of the eight-member ring is 1.09 per square nanometer and that the average distance between the center of the eight-member rings is about 9.0 Å. This large separation of the eight-member rings in AG can be useful for the applications of single-atom catalysis.

Figure 3 shows the calculated total and partial density of states for the free-standing pristine graphene and AG. We find that the electronic states near the Fermi level originate entirely from the p_z orbitals. Unlike pristine graphene, AG exhibits many peaks around the Fermi level, reflecting disorder-derived electron localizations. This electron localization phenomenon of AG not only explains the more covalent character of the Ni–C bond on AG (or shorter $d_{\text{Ni–C}}$) than on pristine graphene, but also induces a partial preservation of spin moment of Ni adatoms on AG, as discussed below.

To examine the covalent character of the Ni–C bond of Ni adatoms on AG and graphene, we calculate the charge-density difference, defined as

$$\Delta\rho = \rho_{\text{total}} - \rho_{\text{substrate}} - \rho_{\text{adsorbate}}, \quad (2)$$

where ρ_{total} is the charge density of the whole adsorbate–substrate system; $\rho_{\text{adsorbate}}$ and $\rho_{\text{substrate}}$ are the charge densities of separated adsorbate and substrate, respectively.

Figures 4(a) and 4(b) show $\Delta\rho$ for the most stable adsorption configurations of a Ni single atom at the hollow site on pristine graphene and the S_4 site on AG, respectively. We find that $\Delta\rho$ exhibits a more localized character of the Ni–C bond on AG compared to pristine graphene. Therefore, the former bond has a shorter $d_{\text{Ni–C}}$ value of 1.90 Å than the latter one (2.10 Å). Similarly, for an adsorbed Ni dimer parallel to the substrate, we find a more covalent character of the Ni–C bond at the D_4 site on AG [see Figs. 4(c) and 4(d)], which results in a shorter $d_{\text{Ni–C}}$ value of 2.01 Å than that (2.13 Å) at the D_g site on pristine graphene.

B. Spin preservation of Ni single atom and dimer adsorbed on AG

We calculate the magnetic moments of a Ni single atom and dimer adsorbed on pristine graphene and AG. For a Ni single atom adsorbed on pristine graphene, the hollow site of the six-member ring is the most stable adsorption site. This hollow site and other local minimum adsorption sites, including “off the hollow site” and “at the hollow site on the nonrelaxed pristine graphene,” have a nonmagnetic ground state: i.e., any initial magnetic moment of Ni adatom converges to zero. It is thus likely that the adsorption sites of a Ni single atom on pristine graphene do not affect the nonmagnetic property. Meanwhile, for the adsorption of a Ni single atom on AG, the bridge site in the eight-member ring is the most stable adsorption site. Due to the complex structure of AG, there are multiple local minima such as the hollow sites

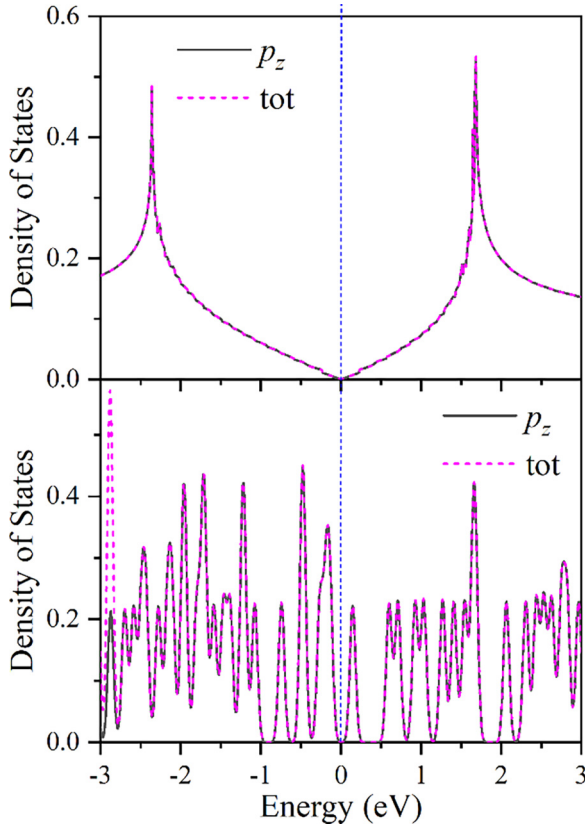


FIG. 3. Calculated the DOS of the free-standing (a) pristine graphene and (b) AG. The unit of DOS is states per eV per primitive unit cell of pristine graphene. The partial DOS for p_z orbital is also given.

of pentagons and hexagons, the hollow sites that are slightly off the center of the seven-member ring, and the bridge sites of the five-, six-, and seven-member rings (see Table I). Although the calculated Ni magnetic moments vary depending on the adsorption sites, the spin preservation of a Ni single atom on AG remains intact, as discussed below.

We compare the calculated magnetic moments of a Ni single atom at the hollow site on pristine graphene and the bridge site of the eight-member ring on AG. While the magnetic moment of a Ni single atom on pristine graphene is absent, that on AG becomes $0.54 \mu_B$. Here, the magnetic moment of the AG sheet is $-0.29 \mu_B$, indicating that the spin moments of Ni adatom and AG substrate are antiferromagnetically coupled with each other. Therefore, the Ni single atom adsorbed at the bridge site on AG has a total magnetic moment of $0.25 \mu_B$. For an adsorbed Ni dimer lying parallel to the substrate, pristine graphene completely loses the magnetic moment, while AG has 0.63 and $0.85 \mu_B$ for two Ni atoms and $0.05 \mu_B$ for the substrate (see Table II). The resultant total magnetic moment of $1.53 \mu_B$ for an adsorbed Ni dimer is much larger than that ($0.25 \mu_B$) for an adsorbed Ni single adatom on AG. Furthermore, the total magnetic moment for an adsorbed Ni dimer perpendicular to the AG sheet increases to $2.02 \mu_B$ (see Table II). Interestingly, as shown in Table II, the magnetic moment of an adsorbed Ni dimer perpendicular to pristine graphene is close to that of the corresponding Ni dimer on

TABLE II. Calculated magnetic moments (in μ_B) of Ni single atom and dimer on AG and PG. Here, m_{Ni1} is the magnetic moment of Ni_1 atom attached to the substrate and m_{Ni2} is the magnetic moment of Ni_2 atom. For Ni dimer adsorbed on AG/PG vertically, Ni_2 atom is one away from the substrate, m_s is the magnetic moment of substrate, and m_t is the total magnetic moment.

	Site	m_{Ni1}	m_{Ni2}	m_s	m_t
Single/AG	Bridge	0.54		-0.29	0.25
Single/PG	Hollow	0.00		0.00	0.00
Dimer(P)/AG	D_4	0.63	0.85	0.05	1.53
Dimer(P)/PG	D_g	0.00	0.00	0.00	0.00
Dimer(V)/AG	Bridge	0.83	1.26	-0.07	2.02
Dimer(V)/PG	Hollow	0.76	1.26	-0.01	2.01

AG. This emergence of magnetic moment in adsorbed Ni dimer on pristine graphene can be explained by a weakened hybridization between the d orbitals of the Ni_1 atom (attached to C) and the π orbital of graphene, as discussed below. It is worth noting that the magnetic moment of Ni_1 is smaller than that of the Ni_2 atom (away from the substrate), indicating that the hybridization of Ni_1 with the substrate weakens the magnetic moment (see Table II).

Early angle-resolved photoemission measurements for the graphene/Ni(111) heterostructure reported that the magnetic moment of Ni surface atoms is suppressed as compared to a clean Ni(111) surface [37,38]. This suppressed spin polarization of Ni surface atoms in the graphene/Ni(111) heterostructure was explained by the hybridization between Ni d - and graphene π orbitals. Such a $p-d$ hybridization was revealed to accompany charge transfer from Ni surface atoms to the graphene layer [37]. We note that our DFT calculations for an isolated Ni atom obtain the electronic configuration of $3d^{8.89}4s^{1.11}$ with a spin moment of $2 \mu_B$, in good agreement with previous DFT calculations [21,39]. It is thus likely that the charge transfer from Ni adatoms to pristine graphene occurs effectively, thereby leading to a zero-spin moment. Meanwhile, such a charge transfer on AG is hindered due to the local disorder around the adsorption sites of AG (see Fig. 3), which renders spin preservation in Ni adatoms, as discussed below.

Disorders in solid materials can be categorized into two types: i.e., compositional and structural (topological) disorders. AG is in the category of structural disorder. Although carbon atoms in AG are displaced from their average equilibrium positions in pristine graphene, the coordination number, average bond length, and average bond angles are maintained to be almost identical to those of pristine graphene. The tight-binding model is the conventional choice for dealing with disordered solid materials [40,41]. The Hamiltonian for a disordered system can be approximately expressed by

$$\begin{aligned}
 H = & \sum_{k,\sigma} E_k c_{k\sigma}^+ c_{k\sigma} + \sum_{d,\sigma} E_d d_{d\sigma}^+ d_{d\sigma} + \frac{U}{2} \sum_{\sigma} E_{d\sigma} c_{d\sigma}^+ c_{d\sigma} c_{d\bar{\sigma}}^+ c_{d\bar{\sigma}} \\
 & + \sum_{k,d} V_{kd} (c_{k\sigma}^+ d_{d\sigma} + d_{d\sigma}^+ c_{k\sigma}). \quad (3)
 \end{aligned}$$

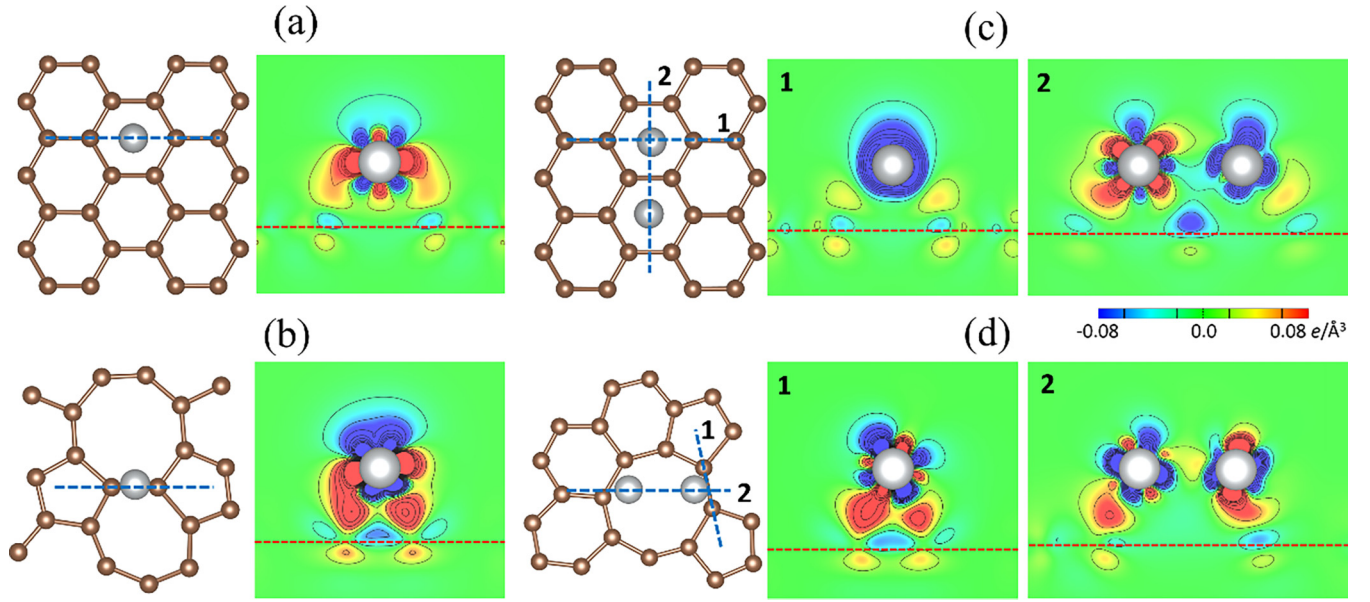


FIG. 4. Calculated charge-density differences $\Delta\rho$ for Ni single adsorbed on (a) pristine graphene and (b) AG. $\Delta\rho$ for Ni dimer adsorbed on pristine graphene and AG are displayed in (c) and (d), respectively. For each adsorption configuration, $\Delta\rho$ is drawn on the vertical plane indicated by the blue dashed line, with a contour spacing of $0.04 e/\text{\AA}^3$. The red dashed lines represent the position of the pristine graphene or AG sheet.

E_k and E_d are the energy eigenvalues of pristine graphene and adsorbed Ni atom, respectively. $c_{k\sigma}^+$ and $c_{k\sigma}$ are creation and annihilation operators for the electronic states in AG, respectively, where σ represents spin-up “ \uparrow ” or spin-down “ \downarrow ” states and $\bar{\sigma} = -\sigma$. U represents the electron correlation energy and V_{kd} denotes the hybridization strength between the C p_z orbitals and the Ni d orbitals. Using retarded Green’s functions [20], we have

$$\langle\langle d_\sigma | d_\sigma^+ \rangle\rangle = \frac{1}{\hbar\omega - E_{d\bar{\sigma}} - U\langle c_{d\bar{\sigma}}^+ c_{d\bar{\sigma}} \rangle + i\pi V_{kd}^2 \rho_F}. \quad (4)$$

Here, we define $\Gamma = \pi V_{kd}^2 \rho_F$, which is a parameter related to the mixing of graphene p_z - and Ni d electrons. ρ_F is the density state at Fermi level. Then, the average number of electrons for spin up and spin down in the Ni d orbitals can be represented as

$$\langle n_{d\uparrow} \rangle = \frac{\Gamma}{U} \cot \pi \langle n_{d\downarrow} \rangle + \frac{E_F - E_d}{U}, \quad (5)$$

$$\langle n_{d\downarrow} \rangle = \frac{\Gamma}{U} \cot \pi \langle n_{d\uparrow} \rangle + \frac{E_F - E_d}{U}, \quad (6)$$

where E_d is the energy of d orbitals. For $0 \leq (E_F - E_d)/U \leq 1$, we set $(E_F - E_d)/U = 1/2$. Then, we differentiate Eqs. (5) and (6) with respect to $\langle n_{d\uparrow} \rangle$ and $\langle n_{d\downarrow} \rangle$, respectively. The resulting equations are multiplied to give the relation

$$1 = \frac{\Gamma}{U} \left(\frac{\pi}{\sqrt{\sin \pi \langle n_{d\uparrow} \rangle \sin \pi \langle n_{d\downarrow} \rangle}} \right). \quad (7)$$

The critical condition for the transition from the magnetic to the nonmagnetic state is $\langle n_{d\uparrow} \rangle = \langle n_{d\downarrow} \rangle = n_c = 1/2$. By

substituting n_c for $\langle n_{d\uparrow} \rangle$ and $\langle n_{d\downarrow} \rangle$, we have

$$\frac{\pi}{\sin \pi n_c} = \frac{U}{\Gamma} \Rightarrow \frac{\Gamma}{U} = \frac{1}{\pi}. \quad (8)$$

The critical value of Γ/U for the transition between the magnetic and nonmagnetic states is $1/\pi$. For $\Gamma/U > 1/\pi$, we employ the graphical approach [20] to obtain one nonmagnetic solution at $\langle n_{d\uparrow} \rangle = \langle n_{d\downarrow} \rangle = 1/2$. Meanwhile, for $\Gamma/U < 1/\pi$, there exist three possible solutions, i.e., one unstable nonmagnetic solution and two stable magnetic solutions [20]. Here, the presence of magnetic solutions is consistent with our results (see Table II). We note that while Γ is directly related to the interaction between the d electrons of Ni atoms and the p_z electrons of AG, U represents the marginal repulsive energy or correlation energy of Ni atoms [20]. For Ni adatom on pristine graphene, Γ/U is considered larger than $1/\pi$ because of the delocalized nature of p_z (or π) orbitals: i.e., the hybridization strength V_{kd} between the d orbitals of Ni atoms and the p_z orbital of graphene is large. On the other hand, for an Ni adatom on AG, Γ/U becomes less than $1/\pi$ because the disordered lattice of AG can significantly reduce V_{kd} via the local disorder effects. Consequently, while the Ni spin moment on graphene completely vanishes, that on AG is partially preserved.

Based on our DFT results with a simple tight-binding model, we explain the disappearance of the spin moment of Ni adatoms on graphene in terms of the strong hybridization between the Ni d orbitals and the graphene π orbital. Meanwhile, as Ni adatoms adsorb on AG, the local disorder effects derived from disordered lattice weaken the hybridization between the d - and π orbitals, thereby preserving a spin moment in Ni adatoms. Our findings have an important implication that the disordered structure of amorphous materials allows

for the preservation of the spin magnetic moment of adsorbed or doped magnetic atoms.

IV. CONCLUSION

Using first-principles calculations, we investigated the structural and magnetic properties of Ni single atom and Ni dimer on the AG sheet. We found that an adsorbed Ni single atom and dimer are more strongly bound on AG than compared to that on pristine graphene. Specifically, the carbon eight-member ring in AG gives rise to the most stable adsorption site for Ni adatoms. Furthermore, we reveal that when a Ni single atom and dimer adsorb on AG, their magnetic moments can be partially preserved. Meanwhile, on pristine graphene, the magnetic moments of adsorbed Ni single atom and dimer (lying parallel to the substrate) completely vanish. The mechanism of spin preservation (disappearance) of adsorbed Ni adatoms on AG (pristine graphene) can

be understood in terms of the disorder-induced localization and its *s-d* interaction model: i.e., the spin preservation of Ni adatoms on AG can be attributed to the weakened hybridization strength between the Ni *d* orbitals and the graphene π orbital due to structural disorder. Therefore, we propose a practical approach to modulate the spin magnetic moment of adsorbed or doped magnetic atoms via the degree of disorder in amorphous materials.

ACKNOWLEDGMENTS

This work is supported by the National Natural Science Foundation of China (Grant No. 12074099), the Natural Science Basic Research Program of Shaanxi Provincial Department of Science and Technology (Grant No. 2023-JC-QN-0151), and Scientific Research Program Funded by Shaanxi Provincial Education Department (Grant No. 18JK0400).

-
- [1] W. Liu, C. Li, Q. Xu, P. Yan, C. Niu, Y. Shen, P. Yuan, and Y. Jia, Anderson localization in 2D amorphous MoO_{3-x} monolayers for electrochemical ammonia synthesis, *Chem Cat Chem* **11**, 5412 (2019).
- [2] Y. Ren, C. Li, Q. Xu, J. Yan, Y. Li, P. Yuan, H. Xia, C. Niu, X. Yang, and Y. Jia, Two-dimensional amorphous heterostructures of Ag/a-WO_{3-x} for high-efficiency photocatalytic performance, *Appl. Catal. B* **245**, 648 (2019).
- [3] N. Li, J. Peng, P. Zhang, and Y. Yue, Amorphous MXene opens new perspectives, *Adv. Mater.* **35**, 2300067 (2023).
- [4] T. Yuan, Z. Hu, Y. Zhao, J. Fang, J. Lv, Q. Zhang, Z. Zhuang, L. Gu, and S. Hu, Two-dimensional amorphous SnO_x from liquid metal: Mass production, phase transfer, and electrocatalytic CO_2 reduction toward formic acid, *Nano Lett.* **20**, 2916 (2020).
- [5] C. Qiao, M. Xu, S. Wang, C.-Z. Wang, K.-M. Ho, X. Miao, and M. Xu, Structure, bonding nature and transition dynamics of amorphous Te, *Scr. Mater.* **202**, 114011 (2021).
- [6] Y. Shang, Z. Liu, J. Dong, M. Yao, Z. Yang, Q. Li, C. Zhai, F. Shen, X. Hou, L. Wang, N. Zhang, W. Zhang, R. Fu, J. Ji, X. Zhang, H. Lin, Y. Fei, B. Sundqvist, W. Wang, and B. Liu, Ultrahard bulk amorphous carbon from collapsed fullerene, *Nature (London)* **599**, 599 (2021).
- [7] C. T. Toh, H. Zhang, J. Lin, A. S. Mayorov, Y.-P. Wang, C. M. Orofeo, D. B. Ferry, H. Andersen, N. Kakenov, Z. Guo, I. H. Abidi, H. Sims, K. Suenaga, S. T. Pantelides, and B. Özyilmaz, Synthesis and properties of freestanding monolayer amorphous carbon, *Nature (London)* **577**, 199 (2020).
- [8] R. Thapa, C. Ugwumadu, K. Nepal, J. Trembly, and D. A. Drabold, Ab initio simulation of amorphous graphite, *Phys. Rev. Lett.* **128**, 236402 (2022).
- [9] Y. T. Zhang, Y. P. Wang, X. Zhang, Y. Y. Zhang, S. Du, and S. T. Pantelides, Structure of amorphous two-dimensional materials: Elemental monolayer amorphous carbon versus binary monolayer amorphous boron nitride, *Nano Lett.* **22**, 8018 (2022).
- [10] H. Tian, Y. Ma, Z. Li, M. Cheng, S. Ning, E. Han, M. Xu, P.-F. Zhang, K. Zhao, R. Li, Y. Zou, P. Liao, S. Yu, X. Li, J. Wang, S. Liu, Y. Li, X. Huang, Z. Yao, D. Ding, J. Guo, Y. Huang, J. Lu, Y. Han, Z. Wang, Z. G. Cheng, J. Liu, Z. Xu, K. Liu, P. Gao, Y. Jiang, L. Lin, X. Zhao, L. Wang, X. Bai, W. Fu, J.-Y. Wang, M. Li, T. Lei, Y. Zhang, Y. Hou, J. Pei, S. J. Pennycook, E. Wang, J. Chen, W. Zhou, and L. Liu, Disorder-tuned conductivity in amorphous monolayer carbon, *Nature (London)* **615**, 56 (2023).
- [11] H. Y. Zhuo, X. Zhang, J. X. Liang, Q. Yu, H. Xiao, and J. Li, Theoretical understandings of graphene-based metal single-atom catalysts: Stability and catalytic performance, *Chem. Rev.* **120**, 12315 (2020).
- [12] P. Seneor, A. Bernard-Mantel, and F. Petroff, Nano spintronics: When spintronics meets single electron physics, *J. Phys.: Condens. Matter* **19**, 165222 (2007).
- [13] K. Nakada, and A. Ishii, Migration of adatom adsorption on graphene using DFT calculation, *Solid State Commun.* **151**, 13 (2011).
- [14] X. Liu, C. Z. Wang, M. Hupalo, W. C. Lu, M. C. Tringides, Y. X. Yao, and K. M. Ho, Metals on graphene: Correlation between adatom adsorption behavior and growth morphology, *Phys. Chem. Chem. Phys.* **14**, 9157 (2012).
- [15] Y. Tang, Z. Yang, and X. Dai, Trapping of metal atoms in the defects on graphene, *J. Chem. Phys.* **135**, 224704 (2011).
- [16] A. V. Krasheninnikov, P. O. Lehtinen, A. S. Foster, P. Pyykkö, and R. M. Nieminen, Embedding transition metal atoms in graphene: Structure, bonding, and magnetism, *Phys. Rev. Lett.* **102**, 126807 (2009).
- [17] E. Griffin, L. Mogg, G.-P. Hao, G. Kalon, C. Bacaksiz, G. Lopez-Polin, T. Y. Zhou, V. Guarochico, J. Cai, C. Neumann, A. Winter, M. Mohn, J. H. Lee, J. Lin, U. Kaiser, I. V. Grigorieva, K. Suenaga, B. Özyilmaz, H.-M. Cheng, W. Ren, A. Turchanin, F. M. Peeters, A. K. Geim, and M. Lozada-Hidalgo, Proton and Li-ion permeation through graphene with eight-atom-ring defects, *ACS Nano* **14**, 7280 (2020).
- [18] L. Zhang, X. Ren, X. Zhao, Y. Zhu, R. Pang, P. Cui, Y. Jia, S. Li, and Z. Zhang, Synergetic charge transfer and spin selection in CO oxidation at neighboring magnetic single-atom catalyst sites, *Nano Lett.* **22**, 3744 (2022).
- [19] P. W. Anderson, Absence of diffusion in certain random lattices, *Phys. Rev.* **109**, 1492 (1958).

- [20] P. W. Anderson, Localized magnetic states in metals, *Phys. Rev.* **124**, 41 (1961).
- [21] H. Johll, H. C. Kang, and E. S. Tok, Density functional theory study of Fe, Co, and Ni adatoms and dimers adsorbed on graphene, *Phys. Rev. B* **79**, 245416 (2009).
- [22] E. Abrahams, P. W. Anderson, D. C. Licciardello, and T. V. Ramakrishnan, Scaling theory of localization: Absence of quantum diffusion in two dimensions, *Phys. Rev. Lett.* **42**, 673 (1979).
- [23] M. Cheng, H. Chen, and J. Chen, Regulating Anderson localization with structural defect disorder (2023), [arXiv:2303.00997](https://arxiv.org/abs/2303.00997) [cond-mat.dis-nn].
- [24] R. Abou-Chacra, D. J. Thouless, and P. W. Anderson, A self consistent theory of localization, *J. Phys. C: Solid State Phys.* **6**, 1734 (1973).
- [25] P. W. Anderson, D. J. Thouless, E. Abrahams, and D. S. Fisher, New method for a scaling theory of localization, *Phys. Rev. B* **22**, 3519 (1980).
- [26] G. Kresse and J. Furthmüller, Efficient iterative schemes for ab initio total-energy calculations using a plane-wave basis set, *Phys. Rev. B* **54**, 11169 (1996).
- [27] P. E. Blöchl, Projector augmented-wave method, *Phys. Rev. B* **50**, 17953 (1994).
- [28] J. P. Perdew, K. Burke, and M. Ernzerhof, Generalized gradient approximation made simple, *Phys. Rev. Lett.* **77**, 3865 (1996).
- [29] O. Y. Long, G. Sai Gautam, and E. A. Carter, Evaluating optimal U for 3d transition-metal oxides within the SCAN+U framework, *Phys. Rev. Mater.* **4**, 045401 (2020).
- [30] S. L. Dudarev, G. A. Botton, S. Y. Savrasov, C. Humphreys, and A. P. Sutton, Electron-energy-loss spectra and the structural stability of nickel oxide: An LSDA+U study, *Phys. Rev. B* **57**, 1505 (1998).
- [31] S. Nosé, A unified formulation of the constant temperature molecular dynamics methods, *J. Chem. Phys.* **81**, 511 (1984).
- [32] W. G. Hoover, Canonical dynamics: Equilibrium phase space distributions, *Phys. Rev. A* **31**, 1695 (1985).
- [33] H. J. Monkhorst and D. Pack, Special points for Brillouin-zone integrations, *Phys. Rev. B* **13**, 5188 (1976).
- [34] S. Grimme, Semiempirical GGA-type density functional constructed with a long-range dispersion correction, *J. Comput. Chem.* **27**, 1787 (2006).
- [35] G. Henkelman, B. P. Uberuaga, and H. Jónsson, A climbing image nudged elastic band method for finding saddle points and minimum energy paths, *J. Chem. Phys.* **113**, 9901 (2000).
- [36] G. Henkelman and H. Jónsson, Improved tangent estimate in the nudged elastic band method for finding minimum energy paths and saddle points, *J. Chem. Phys.* **113**, 9978 (2000).
- [37] S. Sahu, M. R. Sahoo, A. K. Kushwaha, G. Rout, and S. Nayak, Charge transfer and hybridization effect at the graphene-nickel interface: A tight binding model study, *Carbon* **142**, 685 (2019).
- [38] X. Liu, C. Wang, Y. Yao, W. Lu, M. Hupalo, M. Tringides, and K. Ho, Bonding and charge transfer by metal adatom adsorption on graphene, *Phys. Rev. B* **83**, 235411 (2011).
- [39] E. Moroni, G. Kresse, J. Hafner, and J. Furthmüller, Ultrasoft pseudopotentials applied to magnetic Fe, Co, and Ni: From atoms to solids, *Phys. Rev. B* **56**, 15629 (1997).
- [40] D. Weaire and M. F. Thorpe, Electronic properties of an amorphous solid. I. A simple tight-binding theory, *Phys. Rev. B* **4**, 2508 (1971).
- [41] C. Wang, K. Ho, and C. T. Chan, Tight-binding molecular-dynamics study of amorphous carbon, *Phys. Rev. Lett.* **70**, 611 (1993).